Nanoscale

Accepted Manuscript

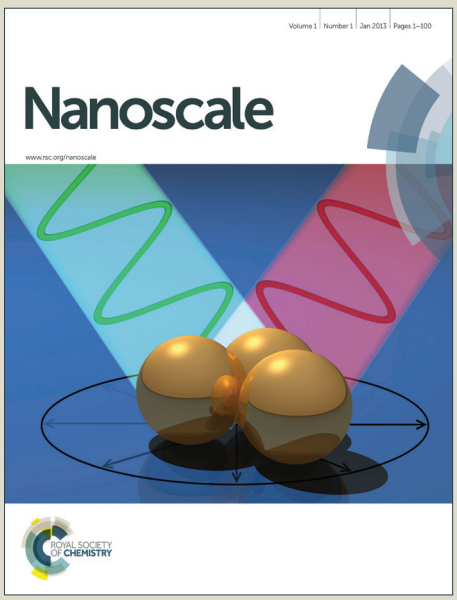

ROYAL SOCIETY OF CHEMISTRY

www.rsc.org/nanoscale

Nanoscale

RSCPublishing

COMMUNICATION

Wafer-scale nanoconical frustum array crystalline silicon solar cells: promising candidates for ultrathin device applications

Cite this: DOI: 10.1039/xoxxoooooox

Received ooth January 2012,
Accepted ooth January 2012

DOI: 10.1039/xoxxoooooox

www.rsc.org/

Yunae Cho,[a] Minji Gwon,[a] Hyeong-Ho Park,[b] Joondong Kim*[c] and Dong-Wook Kim*[a]

High photocurrent of 36.96 mA/cm^2 was achieved for wafer-scaled crystalline Si solar cells with hexagonal nanoconical frustum arrays at the surface. Optical simulations showed that the expected photocurrent of the 10-μm-thick nanostructured cells could slightly exceed the Lambertian limit.

Introduction

Nano-patterning of absorbers enables much improved broadband and omnidirectional light absorption capability, compared with conventional light-trapping strategies, including surface texturing and anti-reflection coatings.[1-29] We demonstrated that surface-patterned crystalline silicon (c-Si) solar cells (diameter: 4 in; thickness ~500 μm), fabricated by nanoimprint lithography, achieved a very high photocurrent of 36.94 mA/cm^2, one of the largest photocurrent values recorded for nanostructured Si solar cells.[1-3] Optical simulations also showed that the surface-concentrated field distribution retained its photocurrent value, as the Si thickness was reduced to 10 μm. This indicates that proper surface patterning enables efficient collection of carriers, as well as photons. Thus, the patterned absorber provides a very versatile approach for realizing high-efficiency ultrathin c-Si solar cells.

c-Si solar cells have dominated in the photovoltaic (PV) market, due to numerous advantages, including superior efficiency, competitive cost to produce electricity, and long-term reliability.[4] Fabrication techniques for commercial c-Si solar cells are now relatively mature. Extensive research on Si-device fabrication for information technology (IT) has accelerated PV-device development. Nowadays, emergent research interest in Si-PV devices is intended for the realization of ultrathin solar cells (less than several tens of microns), led by the rapid development of kerf-less exfoliation processes,[5,6] layer transfer methods,[7,8] integration of stacked Si nanowires,[9] and the fabrication of thin bars and sheets from wafers by anisotropic etching.[10,11] Use of ultrathin Si absorbers further reduces the cost, allowing consolidation of the dominant market share.

Many studies have demonstrated surface nanostructures' beneficial role in light-trapping performance. Considerable experimental effort has been focused on fabrication of high-efficiency, nano-patterned Si solar cells.[1-3,8-18] The measured PV performance of nanostructured cells, however, often cannot surpass those of conventional cells, despite substantially improved optical properties. The optical gain is readily evanescent, due to significant recombination loss from the enlarged surface area.[3,18-20] Very recently, several groups reported the PV characteristics of nano-patterned ultrathin solar cells.[8-11,14-17] The performance results suggest notable potential for high-efficiency, low-cost Si solar cells. Comparative experimental and simulation studies would provide valuable insight into further improvement of nanopatterned Si solar cells for ultrathin device applications.

Results and discussion

Fig. 1 shows six different geometric patterns considered in this study; all patterns consisted of a hexagonal nanoconical frustum array (Fig. 1a and b), which is known to be very efficient for lower optical reflectance over a broad wavelength range.[16,21,22] The top diameter has been shown to be insensitive to the spectral response and, hence, was set to 120 nm.[22] Three different values for the height (H) and bottom diameter (D) were tested, and the resulting optical properties were compared based on numerical calculations (Fig. 1d and e). From previous reports, D values, comparable to the peak wavelength of solar radiation (i.e., visible wavelength) were chosen, to take full advantage of diffraction for efficient light trapping.[22-25] Larger heights (H) can cause significant surface recombination loss; hence, the height was set to <1 μm in this study.[17] The thickness of the underlying Si wafer was set to 10 μm, to examine the potential of the ultrathin device.

Fig. 2a shows the simulated optical reflectance (R) for the six Si nanostructures; each nanostructure configuration included an 80-nm-thick SiN_x surface passivation layer. The optical reflectance of the nanostructures was less than 20% in the visible range, and even less than a few percent over a broad wavelength range. When the nanopattern dimensions were smaller than the wavelength of incident light, the light sees the

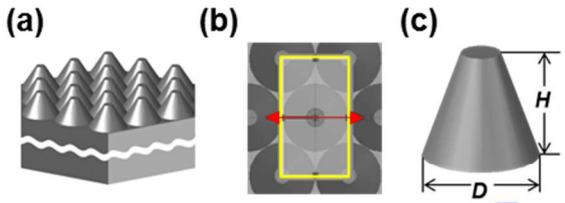

(e)	Nanofrustum Height (*H*)	Bottom Diameter (*D*)
N1	320	200
N2	320	510
N3	320	800
N4	150	510
N5	500	510
N6	700	510

Fig. 1 (a) Architecture of hexagonal nanoconical frustum array solar cells. (b) Top-view of the array: the yellow line and red arrow indicate the unit cell and polarization direction of incident light, respectively, used in optical simulations. (c) A single nanofrustum: *H* and *D* indicate the height and bottom diameter, respectively. The top diameter was fixed at 180 nm. (d) Cross-sectional diagrams illustrating the six patterns used in the calculation. (e) Table of the geometric parameters for the six patterns.

pattern as a uniform medium with a proper dielectric permittivity given by the effective medium approximation.[26] The effective refractive index of the nanopattern will gradually change with variations in the filling fraction, resulting in a drastic reduction in the optical reflection over a broad wavelength range.[2,25,26] Thus, a larger aspect ratio (*H*/*D*), enabling a more graded refractive index (GRI), has lower reflectance. N5 and N6 had a greater height (i.e., aspect ratio) compared with the others, and their reflectance was smaller, as shown in Fig. 2a. In the short wavelength regime, the nanopatterns are no longer perceived as a homogeneous medium; thus, ray optics should be considered in this case. Deinega *et al.* reported that the nano-textured surface with higher aspect ratio should exhibit smaller reflectance due to multiple scattering, based on ray tracing and finite-difference time-domain (FDTD) simulations.[26] Periodic patterns will also work as a refractive diffraction grating. The bottom diameter (*D*) of our patterns, corresponding to the spatial period of the array, determines the optical diffraction of the nanostructures and resulting reflectance spectra. Light, whose wavelength is longer than the period, will be diffracted by gaining a momentum component from the periodic pattern, along the lateral direction.[23] Among our patterns, N1, which had the smallest diameter (200 nm), did not exhibit diffraction over the visible wavelength range. N2 and N3 had identical heights but different bottom diameters. When N2 and N3 were compared, N3 with the larger diameter exhibited light diffraction (into air) over a wide wavelength range; therefore, the reflectance of N3 was larger than that for N2. The oscillatory patterns for long wavelengths (> 800 nm) in the reflectance spectra in Fig. 2a indicated Fabry–Perot-type interference by the 10-μm-thick Si underlayer.

Fig. 2b and 2c show the optical transmission (*T*) and resulting absorption ($A = 1 - R - T$) for the six patterns. The transmission for all patterns was negligible at short wavelengths (< 600 nm), because the penetration depth was shorter than the planar Si-layer thickness (10 μm). At long wavelengths, the physical thickness of Si was less than the light penetration

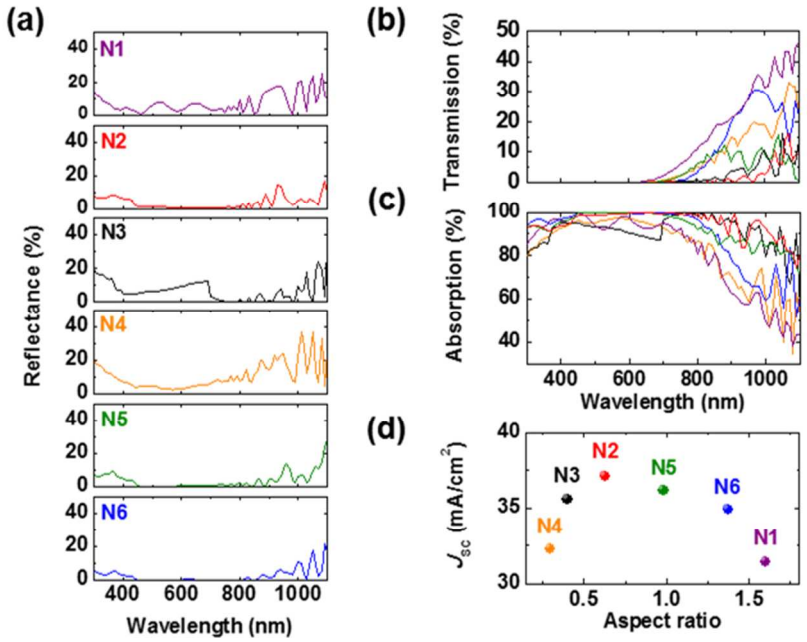

Fig. 2 Calculated optical (a) reflectance (*R*), (b) transmission (*T*), and (c) absorption spectra (*A*) of a 10-μm-thick Si absorber for six surface patterns. (d) Maximum achievable short-circuit current (J_{SC}) of the solar cells having the six surface patterns. In the calculations, the 80-nm-thick SiNx layer on the top surface was used for both passivation and antireflection effects.

depth; hence, the transmission showed considerable variation, which depended on the optical path length enlargement capability of each patterned nanostructure. It should be noted that the pattern showing the lowest optical reflectance (R) did not necessarily show the lowest transmission (T). This indicates that geometric structures showing optimal antireflection effects do not guarantee desirable light-trapping effects in a thin Si absorber.

The influence of surface nanopatterns on optical transmission in a thin Si layer has been reported.[17,21,22,25] Based on calculations, Wang and Leu reported that a large aspect ratio increased transmission loss and limited absorption in their Si nanoconical frustum array, having a height of a few microns.[21] Their results clearly showed a substantial difference in the structural requirements for antireflection and light trapping. Jeong *et al*. reported similar tendencies from their hybrid Si/organic solar cells, with nanoconical array surface patterns; nanocones having an aspect ratio of ~1 provided the best balance between the antireflection effect and light trapping for 10-μm-thick absorbers.[17] They argued that the sub-wavelength surface nanopatterns enabled significant light scattering and lateral light propagation, resulting in superior light trapping in thin absorbers. Wangyang *et al*. and Zhang *et al*. claimed that the diffracted light could undergo total internal reflection (TIR) at the back surface of Si, drastically reducing the transmission loss.[22,25] A larger period broadens the wavelength range undergoing TIR at the back surface, enabling superior light trapping [see Supporting Information, Fig. S1]. Trompoukis *et al*. also claimed that the overall absorption at the surface of the nano-patterned Si thin absorber should be governed by the superposition of the graded refractive index effect and the diffraction of light inside the photoactive layer.[8] Although the geometric parameters were different in this study, due to distinct features in specific cell designs, the results from these previous studies support our results. In this study, the absorption value (A) of N6, with the largest aspect ratio (H/D = 1.4) and the smallest reflectance, was mid-range among the six patterns. In contrast, N2 (H = 320 nm, D = 510 nm, and H/D = 0.63) exhibited the lowest transmission and the largest A (Fig. 2b and c), despite the moderate reflectance shown by the six patterns (Fig. 2a).

For quantitative comparison, maximum achievable short-circuit current density (J_{sc}) of the patterned solar cells can be estimated from the following equation

$$J_{SC} = \int_{300nm}^{\lambda_g} I(\lambda)A(\lambda)\frac{e\lambda}{hc}d\lambda$$

where λ is the wavelength, $I(\lambda)$ is the AM 1.5 solar spectral irradiance, $A(\lambda)$ is the absorption, and λ_g is the wavelength corresponding to the band gap of Si (1100 nm).[29] Fig. 2d shows the estimated J_{sc} values of the six patterns: J_{sc} of N2 was the largest among the six structures, as expected from the absorption spectra in Fig. 2c.

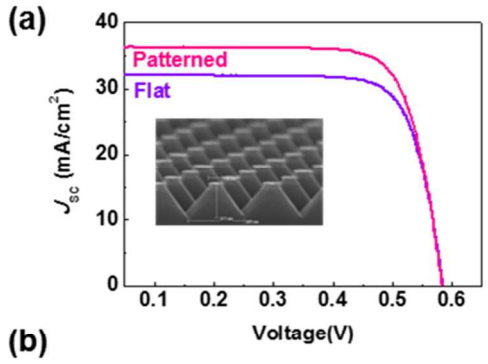

	V_{OC} (V)	J_{SC} (mA/cm^2)	*FF* (%)	Eff. (%)
Flat	0.587	34.02	71.3	14.3
Patterned	0.575	36.96	74.2	15.8

Fig. 3 (a) Current density (J) versus voltage (V) plots of the flat and patterned Si solar cells, prepared by the nanoimprint method using conventional 500-μm-thick wafers, under AM 1.5 illumination conditions. Inset shows a scanning electron microscope (SEM) image of the surface pattern. (b) Photovoltaic characteristics of the flat and patterned cells.

Based on the above calculation, Si solar cells with surface patterns like N2 were fabricated using conventional 500-μm-thick wafers (more details about the fabrication processes are described in the Experimental Section and Supporting Information, Fig. S2). Fig. 3 shows the current density–voltage (J–V) characteristics of the patterned solar cell and a reference flat cell. The nanopatterned solar cell had a higher J_{SC} than the planar cell, due to absorption enhancement, as discussed above. The measured J_{SC} of the patterned cell approached 36.96 mA/cm^2, one of the largest values reported for c-Si solar cells with surface nanopatterns.[1-3] The open-circuit voltage (V_{OC}) of the patterned cell (0.575 V) was slightly smaller than that of the flat reference cell (0.587 V). The patterning of a light absorber generates defects along the surface, readily inducing recombination and often lowering V_{OC}.[3,19,30] One solution is to adopt a shallow-doped emitter layer (profiling the patterned structure), to substantially enlarge the space-charge region (SCR). An existing strong electric field inside the SCR can

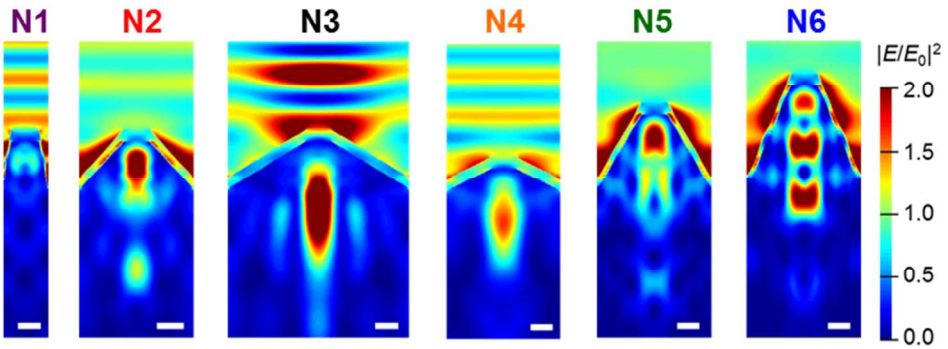

Fig. 4 Electric field distributions near the surface for the six surface patterns. The wavelength of incident light was 550 nm. The scale bar is 100 nm.

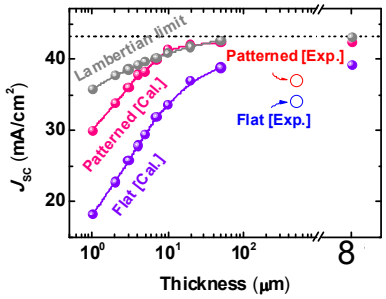

Fig. 5 Calculated photocurrent of the flat and patterned cells as a function of thickness. The maximum photocurrent of the Lambertian limit is also included in the plot.

suppress collection loss of photo-generated carriers.[31,32] Additionally, a further increase in V_{OC} is expected for a thinner Si wafer, where the possibility of Auger recombination loss is minimal.[3,33] Careful device design, including the back contacts and a grid, as well as optimized cell fabrication, is necessary to improve the efficiency of the patterned cell.

Fig. 4 shows the electric field distribution near the top surface region of the six patterns, obtained from FDTD simulations for light having a wavelength of 550 nm. The strong concentration of light near the top surface was remarkable. Additionally, we noted that the region showing the strongest field intensity was located below the surface of the cell, similar to Wang and Leu's report.[21] Excitation of the resonant guided modes in the nanofrustum array, assisted by the aforementioned antireflection and light-trapping effects, should induce such field patterns.[21,24,25] In our patterned cells, the highest photon density was expected to reside near the *p-n* junction, where the built-in potential separates the electron–hole pairs, resulting in very efficient carrier collection.[31,32] All of the results above suggest that our surface patterns played a beneficial role in not only enhancing optical absorption but also improving carrier collection. Combined optical and electrical modeling, recently attempted by some researchers, would be helpful for further efficiency enhancement.[28,29]

The benefits of the nanopatterned surface are clearly shown in the plot of J_{SC} versus absorber thickness in Fig. 5. The J_{SC} of the patterned cells was compared with those obtained from the flat absorber and Lambertian limit.[13] For the flat sample, J_{SC} continuously decreased as the absorber thickness decreased; a rapid drop in J_{SC} was observed for an absorber thickness of a few tens of microns, indicating serious absorption loss. In the patterned cells, the reduction in J_{SC} was minimal as the absorber thickness decreased to a few tens of microns; this was attributed to the superior light-trapping capability of the nanopatterns, as discussed above. The Lambertian limit demonstrated superior photocurrent gain over the entire thickness range. Notably, the J_{SC} of the 10-μm thick pattern slightly exceeded that of the Lambertian limit. The experimental data for 500-μm-thick wafers are smaller than the calculation results, which should be caused by recombination loss.[3,18-20]

Fig. 6 shows a comparison of the spectral irradiance a surface nanopattern (N2), and Lambertian light trapping. The nanopatterned solar cell exhibited the largest optical absorption, exceeding the Lambertian limit at a wavelength >1 μm. The spatial distribution of the electric field clearly showed intensity modulation (i.e., nodes and antinodes) along the lateral direction. This indicates the horizontal propagation of light and

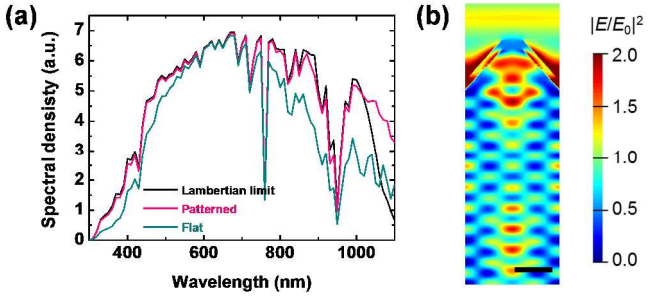

Fig. 6 (a) Calculated spectral irradiance absorbed by the 10-μm-thick Si absorbers having a flat surface, a surface nanopattern (N2), and Lambertian light trapping. (b) Spatial distribution of normalized electric field intensity, $|\boldsymbol{E}/\boldsymbol{E}_0|^2$ ($\boldsymbol{E}_0$: electric field of the incident light), in the nanopattern, for a wavelength of 980 nm. The scale bar is 100 nm.

remarkable enlargement of the optical thickness of the nanopatterned absorber, even under light irradiation at normal incidence. Such superior light trapping capability explains the improved absorption spectra of patterned 10-μm-thick Si absorbers (also see the field profiles of other patterns in Supporting Information, Fig. S3). If the absorber thickness is reduced (e.g., from 10 μm to 1 μm), smaller number of the guide modes and evanescent wave will limit the absorption gain. Thus, J_{SC} of the patterned cell drops, as shown in Fig. 5.

Conclusions

In this study, a very large photocurrent of 36.96 mA/cm^2, one of the largest photocurrents recorded for nanostructured cells, was demonstrated for 4-in-diameter 500-μm-thick c-Si solar cells, having hexagonal nanoconical frustum array surface patterns. The samples were prepared using an ultraviolet (UV) nanoimprint method. Optical simulations of patterned solar cells exhibited significantly enhanced optical absorption via antireflection and light-trapping effects; optical gain was maintained, as the absorber thickness was reduced to 10 μm. The expected photocurrent of the 10-μm-thick cell slightly exceeded the Lambertian limit, due to the increase in absorption for light having a wavelength >1 μm. These results suggest nanopatterned structures as strong candidates for ultrathin c-Si solar cell applications.

Experimental Section

Fabrication of *p-n* junctions: *p-n* junction solar cells were fabricated by conventional processes. An emitter layer (*n*-Si) was formed on a Chokralsky (CZ) grown 4-inch *p*-type (100) Si wafer, having a resistivity of 1–10 Ω cm. Phosphoryl chloride ($POCl_3$) was used as the doping agent, which flowed in a furnace at 800°C for 40 min. The phosphosilicate glass (PSG) that formed during the doping step was removed by buffered hydrofluoric acid (10 wt% HF).

Fabrication of nanopatterns: For the cells with surface nanopatterns, polymethyl methacrylate (PMMA) nanostructures were formed using the UV-imprint method on a *p*-type Si wafer. A wet-etching process, using HF/HNO_3 (volume ratio: 1:19) as the etching solution, etched the Si area not covered by the PMMA nanostructures. Such an etching process produces isotropic-reacting Si for nanofrustum array formation. After

removing the PMMA remains, an emitter layer (n-type Si) was formed using a similar technique to that for a planar cell.

Solar cell device fabrication: On both planar and patterned cells, 80-nm-thick SiN_x passivation layers were deposited by plasma-enhanced chemical vapor deposition. Back contact formation was achieved using a print screen of Al paste (Ferro 53-102). In order to establish the back-surface field region, thermal treatment was performed in a belt furnace at 760 °C with a speed of 160 inch per minute (IPM). For the front contact, Ag paste (Ferro 33-462) was screen-printed onto the top.

Characterizations of solar cells: Current–voltage (*I–V*) characteristics of the devices in the dark were investigated using a semiconductor parameter analyzer (HP 4156B). Photovoltaic measurements were carried out using a sourcemeter (Keithley 2400) and a solar simulator system (McScience K3000). The optical reflectance of the sample was studied using an UV-visible spectrophotometer (V-570, JASCO) with an integrating sphere.

Optical simulations: To understand the optical characteristics of the solar cells, Maxwell's equations were numerically solved using the FDTD method (Lumerical FDTD Solutions). The devices were modeled with unit cells and the associated boundary conditions.

Acknowledgements

This work was supported by Korea Institute of Energy Technology Evaluation and Planning Grant funded by the Ministry of Trade, Industry and Energy (KETEP-20133030011000). Y.J., M.G., and D.-W. K. were also supported by the Quantum Metamaterials Research Center (NRF-2008-0061893) through the National Research Foundation of Korea Grant funded by the Ministry of Science, ICT & Future Planning. The supporting information is available online from Wiley InterScience or from the author.

Notes and references

[a] Department of Physics, Ewha Womans University, Seoul, 120-750, Republic of Korea. *E-mail: dwkim@ewha.ac.kr
[b] Nano Process Division, Korea Advanced Nano Fab Center (KANC), Suwon, 443-270, Republic of Korea.
[c] Department of Electrical Engineering, Incheon National University, Incheon, 406-772, Republic of Korea. *E-mail: joonkim@incheon.ac.kr

Electronic Supplementary Information (ESI) available: See DOI: 10.1039/c000000x/

1 K.-Q. Peng, X. Wang, L. Li, X.-L. Wu and S.-T. Lee, *J. Am. Chem. Soc.,* 2010, **132**, 6872.
2 Y. Li, H. Yu, J. Li, S.-M. Wong, X. W. Sun, X. Li, C. Cheng, H. J. Fan, J. Wang, N. Singh, P. G.-Q. Lo and D.-L. Kwong, *Small*, 2011, **7**, 3138.
3 J. Oh, H.-C. Yaun and H. M. Branz, *Nat. Nanotechnology,* 2012, **7**, 743.
4 A. Goodrich, P. Hacke, Q. Wang, B. Sopori, R. Margolis, T. L. James and M. Woodhouse, *Sol. Energy Mater. Sol. Cells*, 2013, **114**, 110.
5 D. M. Powell, J. Hofstetter, D. P. Fenning, R. Hao, T. S. Ravi and T. Buonassisi, *Appl. Phys. Lett*., 2013, **103**, 263902.
6 S. Saha, M. M. Hilali, E. U. Onyegam, D. Sarkar, D. Jawarani, R. A. Rao, L. Mathew, R. S. Smith, D. Xu, U. K. Das, B. Sopori and S. K. Banerjee, *Appl. Phys. Lett*., 2013, **102**, 163904.
7 J. H. Petermann, D. Zielke, J. Schmidt, F. Haase, E. G. Rojas and R. Brendel, *Prog. Photovolt: Res. Appl*., 2012, **20**, 1.
8 C. Trompoukis, O. E. Daif, V. Depauw, I. Gordon and J. Poortmans, *Appl. Phys. Lett*., 2012, **101**, 103901.
9 T. J. Kempa, J. F. Cahoona, S.-K. Kim, R. W. Day, D. C. Bell, H.-G. Park and C. M. Lieber, *Proc. Natl. Acad. Sci. U.S.A*., 2012, **109**, 1407.
10 K. J. Yu, L. Gao, J. S. Park, Y. R. Lee, C. J. Cocoran, R. G. Nuzzo, D. Chanda and J. A. Rogers, *Adv. Energy Mater*., 2013, **3**, 1401.
11 A. Mavrokefalos, S. E. Han, S. Yerci, M. S. Branham and G. Chen, *Nano Lett*., 2012, **12**, 2792.
12 X. Meng, V. Depauw, G. Gomard, O. E. Daif, C. Trompoukis, E. Drouard, C. Jamois, A. Fave, F. Dross, I. Gordon and C. Seassal, *Opt. Express*, 2012, **20**, A465.
13 A. Bozzola, M. Liscidini and L. C. Andreani, *Opt. Express*, 2012, **20**, A224.
14 S. Jeong, E. C. Garnett, S. Wang, Z. Yu, S. Fan, M. L. Brongersma, M. D. McGehee and Y. Cui, *Nano Lett*., 2012, **12**, 2971.
15 S. Wang, B. D. Weil, Y. Li, K. X. Wang, E. Garnett, S. Fan and Y. Cui, *Nano Lett*., 2013, **13**, 4393.
16 Y. Lu and A. Lal, *Nano Lett*., 2010, **10**, 4651.
17 S. Jeong, M. D. McGehee and Y. Cui, *Nat. Commun*., 2013, **4**, 2950.
18 E. C. Garnet and P. Yang, *J. Am. Chem. Soc*., 2008, **130**, 9224.
19 E. Lee, Y. Kim, M. Gwon, D.-W. Kim, S.-H. Baek and J. H. Kim, *Sol. Energy Mater. Sol. Cells*, 2012, **103**, 93.
20 B. M. Kayes, H. A. Atwater and N. S. Lewis, *J. Appl. Phys*., 2005, **97**, 114302.
21 B. Wang and P. W. Leu, *Nanotechnology,* 2012, **23**, 194003.
22 P. Wangyang, Q. Wang, K. Hu and X. Shen, *Opt. Commun*., 2014, **310**, 19.
23 S. Mokkapati and K. R. Catchpole, *J. Appl. Phys*., 2012, **112**, 101101.
24 S.-K. Kim, K.-D. Song and H.-G. Park, *Opt. Express*, 2012, **20**, A997.
25 R. Y. Zhang, B. Shao, J. R. Dong, J. C. Zhang and H. Yang, *J. Appl. Phys*., 2011, **110**, 113105.
26 A. Deinega, I. Valuev, B. Potapkin and Y. Lozovik, *J. Opt. Soc. Am*., 2011, **A 28**, 770.
27 O. L. Muskens, J. G. Rivas, R. E. Algra, E. P. A. M. Bakkers and A. Lagendijk, *Nano Lett*., 2008, **8**, 2638.
28 A. Deinega, S. Eydeman and S. John, *J. Appl. Phys*., 2013, **113**, 224501.
29 M. Deceglie, V. Ferry, A. Alivisators and H. Atwater, *Nano Lett.*, 2012, **12**, 2894.
30 M. Otto, M. Kroll, T. Käsebier, R. Salzer, A. Tünnermann and R. B. Wehrspohn, *Appl. Phys. Lett*., 2013, **100**, 191603.
31 J. Kim, E. Lee, M. Ju, H. Kim, J. Yi, S.-J. Moon, M. S. Hyun and D.-W. Kim, *Opt. Express*, 2013, **21**, A607.
32 H. Kim, J. Kim, E. Lee, D.-W. Kim, J.-H. Yun and J. Yi, *Appl. Phys. Lett*., 2013, **102**, 193904.

33 S. Y. Herasimenka, W. J. Dauksher and S. G. Bowden, *J. Appl. Phys*., 2013, **113**, 013107.

The table of contents entry

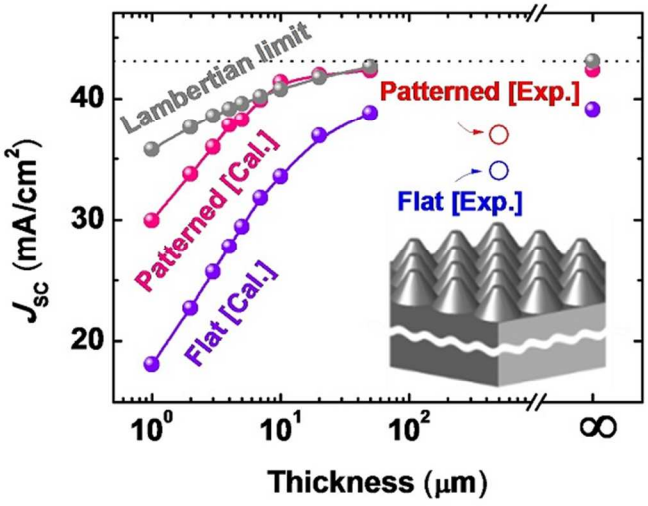

High photocurrent of 36.96 mA/cm^2 was achieved for wafer-scaled crystalline Si solar cells with hexagonal nanoconical frustum arrays at the surface. Optical simulations showed that the expected photocurrent of the 10-μm-thick nanostructured cells could slightly exceed the Lambertian limit.

Keywords: nanoconical frustum arrays, c-Si solar cells, ultrathin devices, nanoimprint

Author: Yunae Cho,[a] Minji Gwon,[a] Hyeong Ho Park,b Joondong Kim,[*c] and Dong-Wook Kim[*a]

Title: Wafer-Scale Nanoconical Frustum Array Crystalline Silicon Solar Cells: Promising Candidates for Ultrathin Device Applications

